

# Using Polar Faculae to Determine the Sun’s High-Latitude Rotation Rate. I. Techniques and Initial Measurements

NEIL R. SHEELEY, JR.<sup>1</sup>

<sup>1</sup>*Visiting Research Scientist  
Lunar and Planetary Laboratory, University of Arizona  
Tucson, AZ 85721, USA*

## ABSTRACT

This paper describes a new way of determining the high-latitude solar rotation rate statistically from simultaneous observations of many polar faculae. In this experiment, I extracted frames from a movie made previously from flat-fielded images obtained in the 6767 Å continuum during February 1997-1998 (Sheeley & Warren 2006) and used those frames to construct space-time maps from high-latitude slices of the favorably oriented south polar cap. These maps show an array of slanted tracks whose average slope indicates the east-west speed of faculae at that latitude,  $\lambda_s$ . When the slopes are measured and plotted as a function of latitude, they show relatively little scatter  $\sim 0.01\text{-}02 \text{ km s}^{-1}$  from a straight line whose zero-speed extension passes through the Sun’s south pole. This means that the speed,  $v(\lambda_s)$ , and the latitudinal radius,  $R_\odot \cos \lambda_s$ , approach 0 at the same rate, so that their ratio gives a nearly constant synodic rotation rate  $\sim 8.6^\circ \text{ day}^{-1}$  surrounding the Sun’s south pole. A few measurements of the unfavorably oriented north polar cap are consistent with these measurements near the south pole.

*Keywords:* Solar faculae (1494)— Solar rotation (1524)—Solar magnetic fields (1503)—Solar cycle (1487)

## 1. INTRODUCTION

The idea for this study occurred on 26 June 2024 when I learned about the COFFIES (Consequences of Fields and Flows in the Interior and Exterior of the Sun) NASA-funded virtual workshop on ‘The Science of the Poles’, organized by Lisa Upton, Shea Hess Webber, and Todd Hoeksema. In that workshop, my work on polar faculae (Sheeley 1964, 1965, 1976, 1991, 2008; Muñoz-Jaramillo et al. 2012) was mentioned. Those studies were about counting polar faculae on white-light images obtained at the Mount Wilson Observatory since 1905 and plotting their evolution over many sunspot cycles. However, in 2006, Harry Warren and I conducted a different study of faculae using images obtained in the 6767 Å continuum during 1996-2005 with the Michelson Doppler Interferometer (MDI) on the *Solar and Heliospheric Observatory* (SOHO) (Sheeley & Warren 2006), and I wondered if that study might be relevant to the polar studies of the COFFIES group too.

Our main objective in that 2006 study was to make Carrington maps that showed the distribution of faculae over the full Sun, similar to Carrington maps of photospheric magnetic fields and the associated Ca II K-line emission seen in Mount Wilson spectroheliograms (Sheeley et al. 2011). However, in that 2006 paper, we included a figure with an online link to a time-lapse movie of the 6767 Å disk. The movie consisted of flat-fielded images<sup>1</sup>, obtained during February 7-21 of each year when the solar  $B_0$  angle was centered around  $-6.8^\circ$  and favored a view of the Sun’s south pole. By running the movie at high speed, the background noise was effectively reduced so that the polar faculae were visible as a ‘cloud of bright points’ waxing and waning with time as the sunspot cycle advanced.

However, it was also easy to see individual faculae moving east-to-west with the solar rotation. I wondered if it would be possible to capture this motion in a space-time map, obtained by placing the slit along a chord in the south polar cap. I wanted to keep the project simple and just measure the speed near the central meridian. I did not want to worry about problems that would arise toward the ends of the slit where the curved latitude lines would bend off a

<sup>1</sup> Jeneen Sommers (Stanford University) had provided those images in a flat-fielded form that showed the faculae without the presence of limb darkening.

straight slit and where the curvature of the solar surface would reduce the ‘sky plane’ speed of faculae (which would happen even for the straight latitude contours that occur when  $B_0 = 0$ ).

To accomplish this feat, I enlisted the help of ChatGPT, first to extract the frames from the movie and then to cut out narrow east-west oriented strips from these images and place them in chronological order. I extracted the images and stored them in a directory manually, which took several hours because I wanted to use all 106 of the images during the February 7-21 intervals of 1997 and 1998. In those years, the polar fields were relatively strong compared to the polar fields around sunspot minima in 2009 and 2020, so that may have been our last opportunity to track the faculae when they were still plentiful. Making the space-time maps was much faster than collecting the frames. It only took a few iterations with ChatGPT to obtain a working program that showed slanted tracks. The sight of those tracks was the first ‘ah-ha’ moment of this study. It was clear that the procedure would work and that success was only a matter of time and ‘fine tuning’ the program. (The second ‘ah-ha’ moment occurred later when I discovered that the plotted data points were well fit by a straight line whose zero-speed extension passed through the Sun’s south pole. Consequently, both the linear speed of the faculae and the radius of their latitude contour would approach zero at the same rate and give a nearly constant synodic rotation speed in the vicinity of the pole.)

This paper is organized as follows: In the next section, I will describe the measurement procedure in detail and show a sample of the resulting space-time maps, obtained with different slits and at different latitudes. A few measurements were obtained in the northern hemisphere despite its unfavorable view from SOHO (located at the L1 point on the Earth-Sun line) in February. Then, in the Results section, I show the speed obtained from the space-time maps and plotted versus the measurement latitudes. Finally, in the last section, I summarize these results and compare them with ground-based measurements obtained by tracking magnetic flux elements with the Mount Wilson magnetograph (Snodgrass 1983) and by tracking individual polar faculae when they were especially plentiful during the years 1952-1954 (Müller 1954) and 1951-1954 (Waldmeier 1955).

## 2. MEASUREMENT TECHNIQUES

### 2.1. *The measurement process*

Figure 1 is a sketch of the south polar cap where most of the measurements were made. The red lines indicate  $60^\circ$ ,  $70^\circ$ , and  $80^\circ$  latitude contours on 14 February when the solar  $B_0$  angle is  $-6.8^\circ$ , and the thin horizontal lines indicate the upper and lower edges of a 7-pixel (20 Mm) slit, in this case centered on the  $70^\circ$  contour. Note that the upper

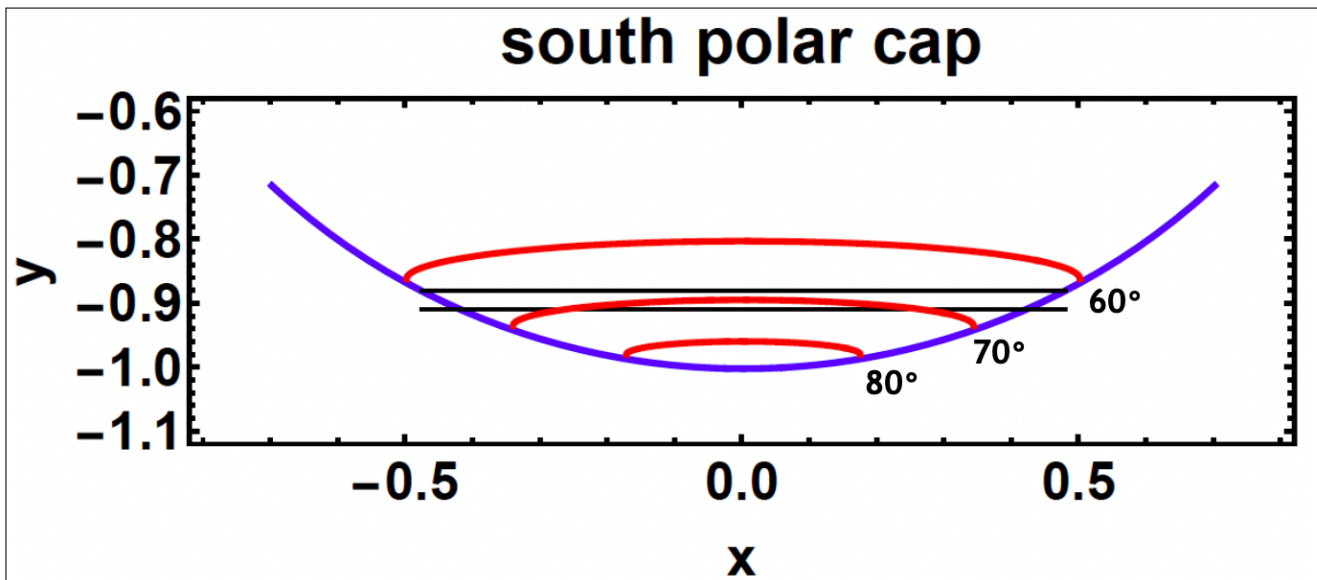


**Figure 1.** Drawing of the south polar cap around 14 February when  $B_0 = -6.8^\circ$  and the south pole is tipped toward Earth (and SOHO). The solar limb is drawn in blue; latitude contours at  $60^\circ$ ,  $70^\circ$ , and  $80^\circ$  are indicated in red; and the upper and lower edges of a sample 7-pixel wide slit are indicated by horizontal black lines. The rectangular coordinate axes,  $x$  and  $y$ , are expressed in units of solar radii.

edge of the slit ends at the solar limb (indicated by the solid blue curve), whereas the lower edge crosses the limb

into the sky background. As the reader will see in the next subsection, this gives the resulting space-time map jagged upper and lower edges. Finally, in reference to Figure 1, the horizontal and vertical dimensions are  $x$  and  $y$  expressed in solar radii with the disk center at  $(0, 0)$  and the southernmost limb at the point  $(0, -1)$ .

However, rectangular distances on the solar image are expressed in pixels with  $(256, 502)$  at the southernmost limb and  $(256, 10)$  at the northernmost limb, and a solar radius of 246 pixels. Consequently, I derived the latitudes of the upper and lower edges of the slit from  $y$ -coordinates measured in pixels and I calculated the chord lengths from  $x$ -coordinates also measured in pixels. In particular, the latitudes were obtained using the relation

$$1 - \frac{(502 - yp_i)}{246} = -y_i = \sin(\lambda_s^{(i)} - 6.8), \quad (1)$$

where  $\lambda_s^{(i)}$  refers to the south latitude of the upper ( $i = 1$ ) or lower ( $i = 2$ ) edge of the slit in degrees,  $y_i$  is the  $y$ -value of that edge of the slit in solar radii,  $yp_i$  is the location of the corresponding edge in pixels, 502 is the  $y$ -value of the southernmost limb in pixels, and 246 is the radius of the solar image in pixels. Finally, I calculated the average,  $\langle \lambda_s \rangle$ , of these two latitudes and used this average as the effective latitude in plots of the speed,  $v(\lambda_s)$ .

I computed the speed by determining how long it would take a given linear track to extend from the row of upper peaks at the east limb to the row of upper peaks at the west limb and then used the relation

$$v = \frac{\Delta x}{\Delta t}, \quad (2)$$

where  $\Delta x$  is the maximum chord length in solar radii given by  $\Delta x = (x_2 - x_1)/246$ , where  $x_1$  and  $x_2$  are the  $x$ -coordinates of the left and right ends of the upper edge of the slit in pixels, and  $\Delta t$ , is the corresponding time difference, obtained from the space-time map.

In practice, this time measurement was done by using a ruler to fit the array of approximately parallel tracks with a straight line and then measuring the horizontal distance that was cut off between the ends of that line in millimeters. This ‘time’ was calibrated in days by comparing the total duration of the map in millimeters with its corresponding interval in days. This interval was 30 days for the 106 frames used in the two intervals 7-21 February 1997 and 7-21 February 1998 because the end dates of 7 February and 21 February were used in both 1997 and 1998. It was important to use the correct time difference (30 days rather than 28 days without the end dates) because its value directly affects the value of the final synodic rotation rate.

An interesting aspect of this unusual movie is that some of the frames in 1997 were not displayed with the same cadence as others. As the mission evolved and more time became available, the cadence increased from a few frames per day in 1997 to a precise routine of 4 frames per day in 1998. In 1997, there were 6 days with 2 frames, 4 days with 3 frames, and 5 days with 4 frames for an average of almost exactly 3 frames per day. So our 30-day interval consisted of 15 days with frames at an average rate of 3 frames per day followed by 15 days with frames at a precise cadence of 4 frames per day. This may have caused some of the tracks to wiggle a little, but it should not have affected the overall calibration of 30 days.

## 2.2. The space-time maps

Figure 2 shows space-time maps obtained at an average latitude of approximately  $76^\circ$  using slit widths  $\Delta y = 5, 7,$  and  $10$  pixels (14, 20, and 28 Mm, respectively). These three panels show the same collection of quasi-parallel tracks that are slanted from the lower left to the upper right. The tabulated speeds of  $0.30 \pm 0.02 \text{ km s}^{-1}$  refer to the slant near the mid-point of the chord and the accuracy of my eye-estimates of their slopes. In addition, the tracks bend horizontally toward the east and west limbs (at the bottom and top of the maps, respectively). This is partly due to the curvature of the Sun’s surface which causes the speed to change from a sky plane motion at the central meridian to a more line-of-sight motion toward the limbs. If the  $B_0$  angle were 0, the latitude contours would be straight lines along the slit. In that case, the speed,  $v$  and  $x$ -position could be described in terms of a longitudinal angle,  $\phi$ , using the equations:

$$v = v_1 \cos \phi \quad (3a)$$

$$x = R_\odot \cos \lambda_s \sin \phi, \quad (3b)$$

where  $v_1$  is the surface speed,  $\lambda_s$  is south latitude, and  $R_\odot$  is the solar radius. Eliminating  $\phi$  between these two equations, we are left with a relation between the speed and the distance along the slit.

$$\frac{v}{v_1} = \sqrt{1 - \left(\frac{x}{R_\odot \cos \lambda_s}\right)^2}. \quad (4)$$

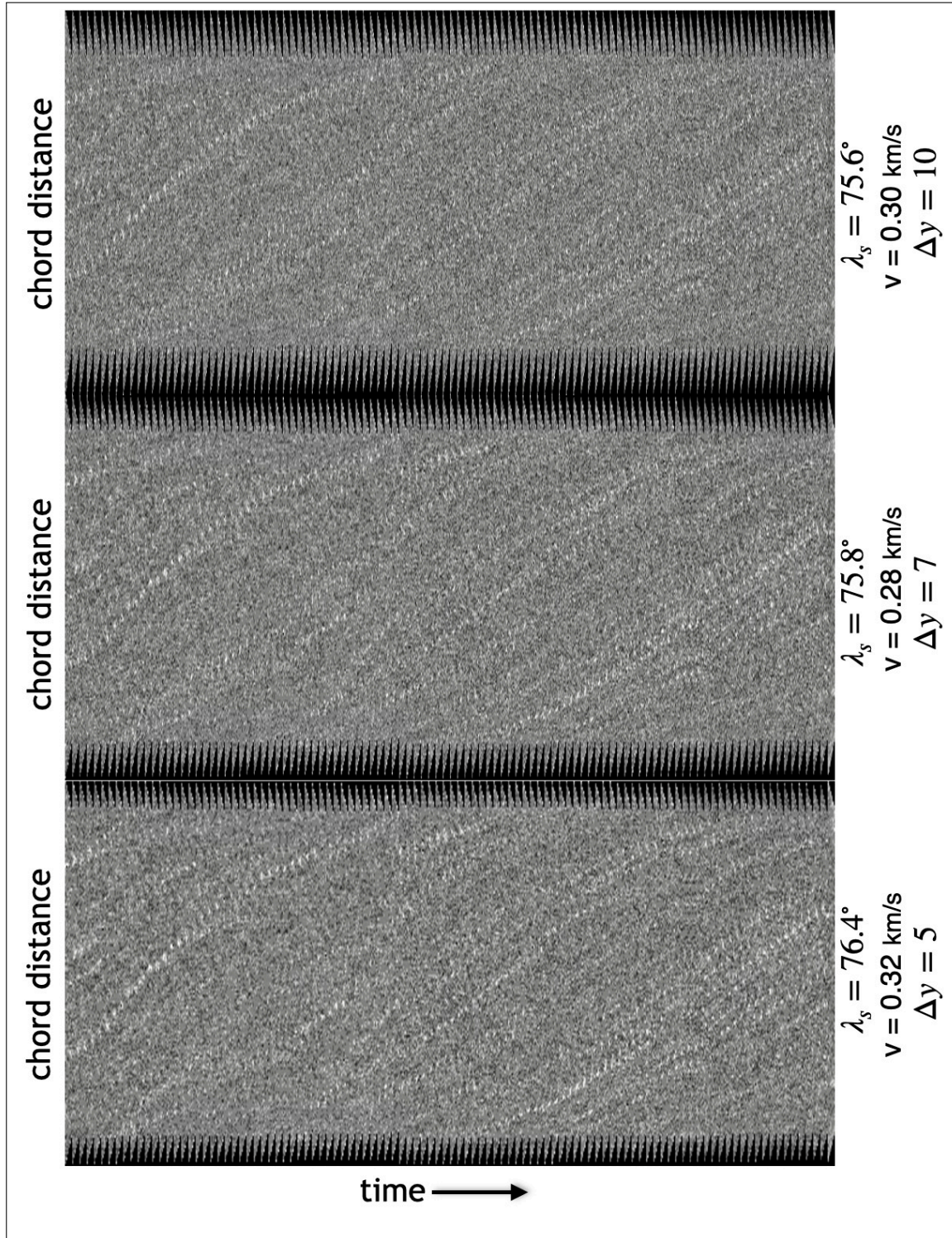


**Figure 2.** Space-time maps obtained at approximately  $76^\circ$  latitude, with slit widths,  $\Delta y = 5, 7,$  and  $10$  pixels (14, 20, and 28 Mm, respectively), showing a greater latitudinal compression and lower resulting contrast of faculae observed with the wider slits. The chord distance is approximately  $2R_\odot \cos(\lambda_s - 6.8^\circ)$  and the time duration is 30 days. The associated speeds are based on eye-estimates of the average inclinations, and their  $\pm 0.02 \text{ km s}^{-1}$  differences reflect the accuracy of those estimates.

Expressing  $x$  and  $v$  in dimensionless units, and recognizing that  $v = dx/dt$ , this equation becomes

$$\frac{dx}{dt} = \sqrt{1 - x^2}, \quad (5)$$

whose solution is simply  $x = \sin t$ . Restoring the units, this solution is

$$\frac{x}{R_{\odot} \cos \lambda_s} = \sin \left( \frac{v_1 t}{R_{\odot} \cos \lambda_s} \right). \quad (6)$$

So, the tracks are simple sine waves whose arguments run from  $-\pi/2$  to  $+\pi/2$ . For  $v_1 t / R_{\odot} \cos \lambda_s \ll \pi/2$ , the solution is  $x = v_1 t$ , and in a space-time map, the tracks would have a constant slope,  $v_1$ , around the mid-point of the chord. However, as the time,  $t$ , increases, and the quantity,  $v_1 t / R_{\odot} \cos \lambda_s$  approaches  $\pi/2$ , the line bends horizontally toward the upper end of the chord where  $x = R_{\odot} \cos \lambda_s$  and  $dx/dt = 0$ . Of course, the antisymmetric behavior occurs in the eastern hemisphere where  $x$  is negative and the curve approaches the lower end of the chord. As mentioned in the previous section, when  $B_0 = -6.8^\circ$ , I ignore the mismatch between the straight slit and the curved latitude profiles, and determine the central speed,  $v_1$ , by extrapolating the linear segment of the track to the top and bottom of the space-time map and divide the chord length by the duration of time,  $\Delta t$ , that is intercepted between the ends of the slit.

Another important characteristic of the space-time maps in Figure 2 is their slit-dependent differences. In order to display these panels with the same 30-day horizontal dimension, it was necessary to compress the 10-pixel slits twice as much as the 5-pixel slits. Likewise, the 7-pixel slits were compressed 1.4 times as much as the 5-pixel slits. This horizontal matching procedure caused the faculae to be narrower in the wider-slit images than in the narrower-slit images. With careful scrutiny, one can see the individual faculae changing from fine, elongated features in the 10-pixel map to rounder features in the 5-pixel map. This compression seems to reduce the contrast of the faculae so that the tracks are visible with greater contrast in the space-time maps made with the narrower slits.

In each map, the time axis spans 30 days with 106 strips whose jagged edges are clearly visible at the top and bottom of the map. As mentioned in the previous subsection, the cadence of these strips is uniform at the rate of 4 strips per day in the second half of the map (1998) and variable at an average rate of about 3 strips per day in the first half of the map (1997). Despite this variable cadence, most of the tracks seem fairly well defined, with steep slopes near the central meridian (the half-chord location) and lower slopes toward the east and west limbs (at the bottom and top of each map).

Figure 3 is a similar comparison using smaller slit widths of  $\Delta y = 3, 5,$  and  $7$  pixels and a larger average latitude at  $80^\circ$  south latitude. The relatively high latitude and narrow slit widths were chosen to increase the visibility of the tracks. In these  $80^\circ$  maps, the tracks seem to have higher contrast than they did at the lower latitude, even when comparing maps of the same slit width. Each panel shows virtually identical patterns of quasi-parallel tracks, moderately steep around the central meridian and shallow toward the limbs. In addition, the tracks seem more fragmentary than in the lower-latitude space-time maps of Figure 2, especially toward the limbs. Presumably, this is a consequence of a greater mismatch between the straight slit and the curved latitude contours at the higher latitude.

Nevertheless, it is still possible to measure their average slope. An eye-estimate of the average mid-latitude slope gives the speeds of  $0.20$ - $0.22 \text{ km s}^{-1}$  shown in the figure, where again the differences reflect the accuracy of those estimates. Clearly, this accuracy is sufficient to show the decrease of speed from  $0.3 \text{ km s}^{-1}$  to  $0.2 \text{ km s}^{-1}$  as the latitude increases from  $76^\circ$  to  $80^\circ$ .

Figure 4 supports this trend by including a third latitude, and provides straight lines as guides for identifying the average slopes. With these space-time maps, the measurement indicates the average contribution of all the faculae and does not depend on tracking a single facula during its relatively short  $\sim 1$ -day lifetime. (In fact, the relatively short lifetimes of individual polar faculae were probably the main reason that 2005 summer student, Hanna Krug, and I had difficulty measuring the high-latitude rotation profile by tracking individual polar faculae on these same SOHO/MDI solar images.) Not only do the white lines decrease their inclinations from the upper panel to the lower panel, but the corresponding speeds decrease from  $0.39 \text{ km s}^{-1}$  at  $\lambda_s = 71.6^\circ$  to  $0.33 \text{ km s}^{-1}$  at  $\lambda_s = 75.2^\circ$ , and finally to  $0.20 \text{ km s}^{-1}$  at  $\lambda_s = 80.2^\circ$ . Next we plot the results for all of our measurements.

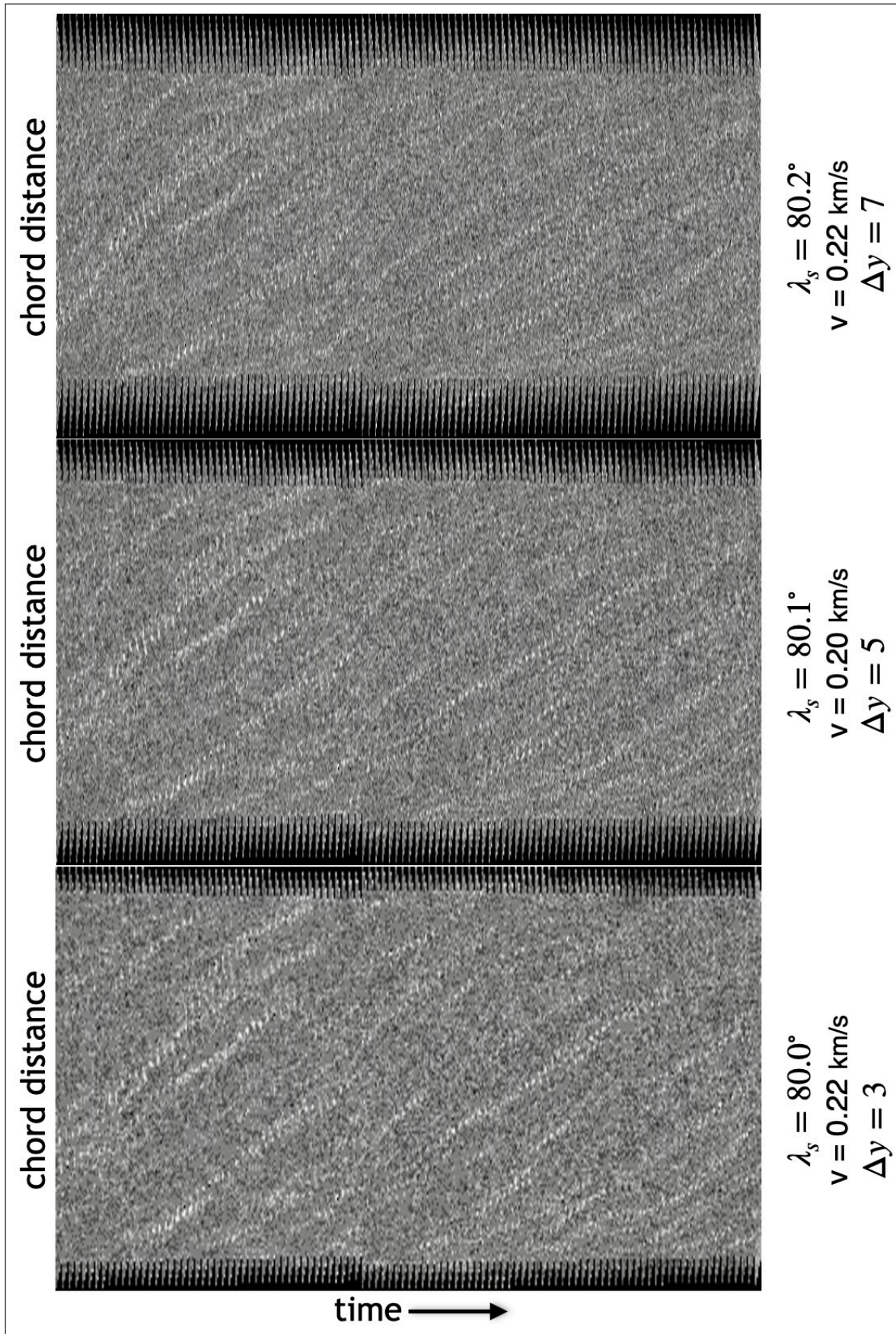


**Figure 3.** Same as Figure 2, except for slit widths,  $\Delta y = 3$ -, 5-, and 7-pixels (8, 14, and 20 Mm, respectively) and a common latitude  $\lambda_s \sim 80^\circ$ , again showing the greater latitudinal compression and decreased contrast obtained with the wider slits.

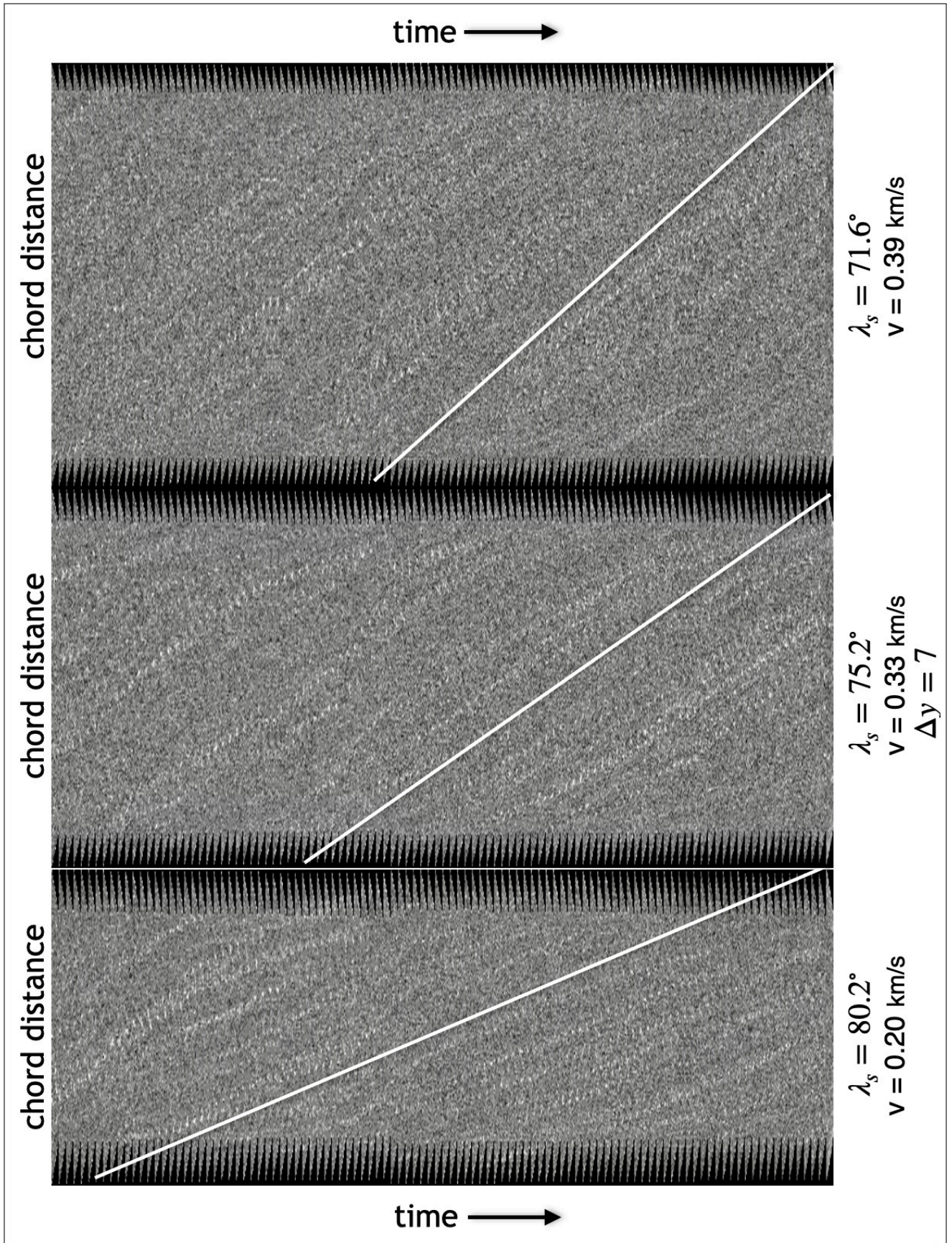


**Figure 4.** Space-time maps obtained using a 7-pixel wide slit (20 Mm) at chords located at  $\lambda_s = 80.2^\circ$ ,  $75.2^\circ$ , and  $71.6^\circ$  south latitude, showing tracks of polar faculae during 7-21 February 1997 and 1998. The lengths of the vertical and horizontal axes are  $\sim 2R_\odot \cos(\lambda_s - 6.8^\circ)$  and 30 days, respectively. White lines are guides for identifying the average slopes of the tracks.

## 3. RESULTS

Figure 5 shows a plot of tracking measurements from space-time maps like those in Figures 2-4, except that the measurements were obtained using a relatively wide 10-pixel slit, corresponding to about 28 Mm. In each case, the latitude refers to the average latitude of the upper and lower edge of the slit. The data points were fit differently in the left and right panels of Figure 5. In the left panel, the red dashed line indicates the usual 2-parameter best fit, and leads to the values of the slope ( $1.54 \text{ km s}^{-1}$ ) and polar intercept ( $0.082 \text{ km s}^{-1}$ ), as indicated by the formula

$$\frac{(v - 0.082)}{1.54} = -\frac{(\lambda_s - 90)}{90}, \quad (7)$$

where  $\lambda_s$  is the south latitude in degrees; the velocity,  $v$ , and fit parameters are in  $\text{km s}^{-1}$ . Also, the rms deviation of this line from the measured speeds is given as  $0.0180 \text{ km s}^{-1}$ . So the fit is fairly good, but the line does not pass through the point at  $(90,0)$ , indicated by the small black circle.

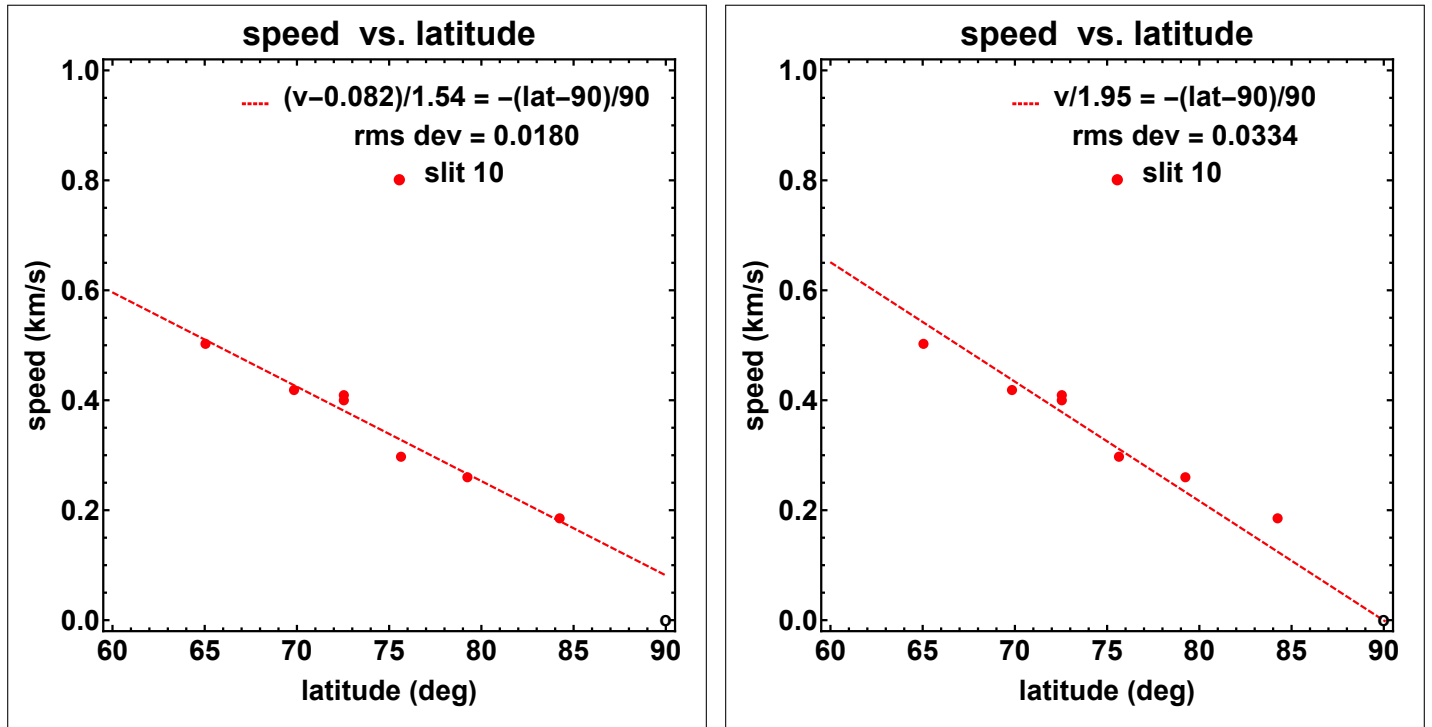


**Figure 5.** Speed versus latitude for measurements obtained with a 10-pixel slit (28 Mm). (left): a 2-parameter straight-line fit for slope and polar speed; (right): a 1-parameter fit for the slope of a line passing through the point  $(90,0)$ . The rms deviations are  $\sim 0.02 \text{ km s}^{-1}$  and  $\sim 0.03 \text{ km s}^{-1}$ , respectively, but the slope is steeper when the speed is forced to vanish at the pole.

The terminology is the same in the right panel, but the straight line is determined differently. The line is forced to pass through the black circle at the point  $(90,0)$ , and the slope of the line is taken as the single, best-fit parameter. The result is

$$\frac{v}{1.95} = -\frac{(\lambda_s - 90)}{90}, \quad (8)$$

and the amount of scatter is  $0.0334 \text{ km s}^{-1}$ , slightly larger than  $0.0180 \text{ km s}^{-1}$  obtained with the 2-parameter fit in the left panel. An important contribution of this forced polar fit is to increase the value of the speed parameter from  $1.54 \text{ km s}^{-1}$  to  $1.95 \text{ km s}^{-1}$ . This has a significant effect on the resulting synodic rotation speed, as we will see below.

Although this result with the 10-pixel slit seems pretty good, it is not as good as I obtained using smaller slits. Figure 6 shows a similar result using slit widths of 7, 5, and 3 pixels ( $\sim 20 \text{ Mm}$ ,  $14 \text{ Mm}$ , and  $8 \text{ Mm}$ , respectively). These measurements are indicated by red points, blue points, and a single green point for the 3-pixel slit. In this case, the left and right panels give comparable amounts of scatter ( $0.023 \text{ km s}^{-1}$  compared to  $0.025 \text{ km s}^{-1}$ ), with a ‘polar intercept’ of  $0.03 \text{ km s}^{-1}$ . When the speed is forced to vanish at the pole, the speed parameter increases from  $1.73 \text{ km s}^{-1}$



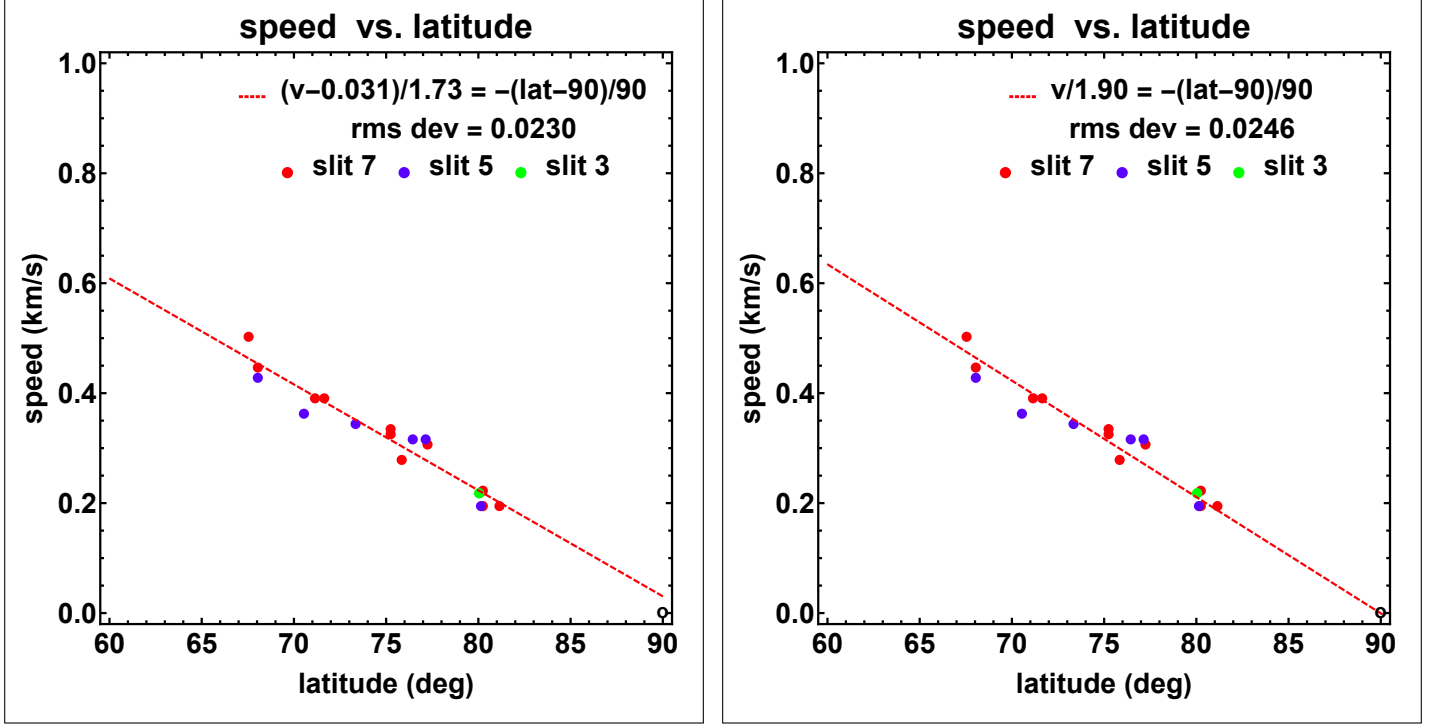


**Figure 6.** Same as Figure 5, but with narrower slits (7-, 5-, and 3-pixel widths are indicated by red, blue, and green points, respectively). With these narrower slits, the 2-parameter fit projects to  $0.03 \text{ km s}^{-1}$  at the pole with an rms deviation of  $0.023 \text{ km s}^{-1}$ , which is slightly smaller than the  $0.025 \text{ km s}^{-1}$  deviation obtained when the speed is forced to vanish at the pole.

$\text{s}^{-1}$  to  $1.90 \text{ km s}^{-1}$  as shown here:

$$\frac{v}{1.90} = -\frac{(\lambda_s - 90)}{90}. \quad (9)$$

Finally, Figure 7 shows the same data with the addition of 3 points obtained in the north polar cap with a 5-pixel slit. These northern-hemisphere points lie in range of  $60\text{-}70^\circ$ , which is systematically lower than the range obtained for the southern-hemisphere points due to the unfavorable view of the north polar region during 7-21 February. In practice, when I calculated the linear offset from the polar limb, I obtained  $\sin(\lambda_s - 6.8)$  in the south and  $\sin(\lambda_n + 6.8)$  in the north. Thus, for the same offset, it was necessary to add  $6.8^\circ$  in the south and subtract  $6.8^\circ$  in the north, making the northern-hemisphere latitude range about  $13.6^\circ$  lower than the southern-hemisphere range. This had the effect of extending the latitude range of the measurements to slightly lower latitudes and slightly reducing the 2-parameter rms scatter from  $0.023$  to  $0.022 \text{ km s}^{-1}$ . Also, the speed parameter of the forced fit decreased slightly from  $1.90$  to  $1.86 \text{ km s}^{-1}$ . This was a relatively minor change; probably the most that we can conclude from this comparison is that the north polar-cap measurements are consistent with the south polar-cap measurements, as one might expect if the two polar regions have the same rotation rate.

Based on these measurements, we conclude that the high-latitude linear speed,  $v$ , is given by an expression of the form

$$\frac{v(\lambda_s)}{v_0} = -\frac{(\lambda_s - \pi/2)}{\pi/2}, \quad (10)$$

where  $v_0 \approx 1.90 \pm 0.05 \text{ km s}^{-1}$ , and  $\lambda_s$  is south latitude, expressed in radians. As I mentioned in the Introduction, the significance of this relation is that  $v(\lambda_s)$  and  $\cos \lambda_s$  have the same  $\lambda_s$ -dependence close to the south pole. This means that their ratio, and thus the angular rotation rate,  $\omega$ , is constant close to the pole. In particular,

$$\omega = \frac{v(\lambda_s)}{R_\odot \cos \lambda_s} = \frac{v_0(2/\pi)(\pi/2 - \lambda_s)}{R_\odot \sin(\pi/2 - \lambda_s)} \approx \frac{2}{\pi} \frac{v_0}{R_\odot}, \quad (11)$$

when  $(\pi/2 - \lambda_s) \ll 1$ . Substituting  $v_0 = 1.90 \text{ km s}^{-1}$  and  $R_\odot \approx 0.7 \times 10^6 \text{ km}$ , and converting from radians to degrees, I get  $\omega \approx 8.6^\circ \text{ day}^{-1}$  as the synodic rotation rate of the south polar cap. The sidereal rate would be about  $1^\circ \text{ day}^{-1}$

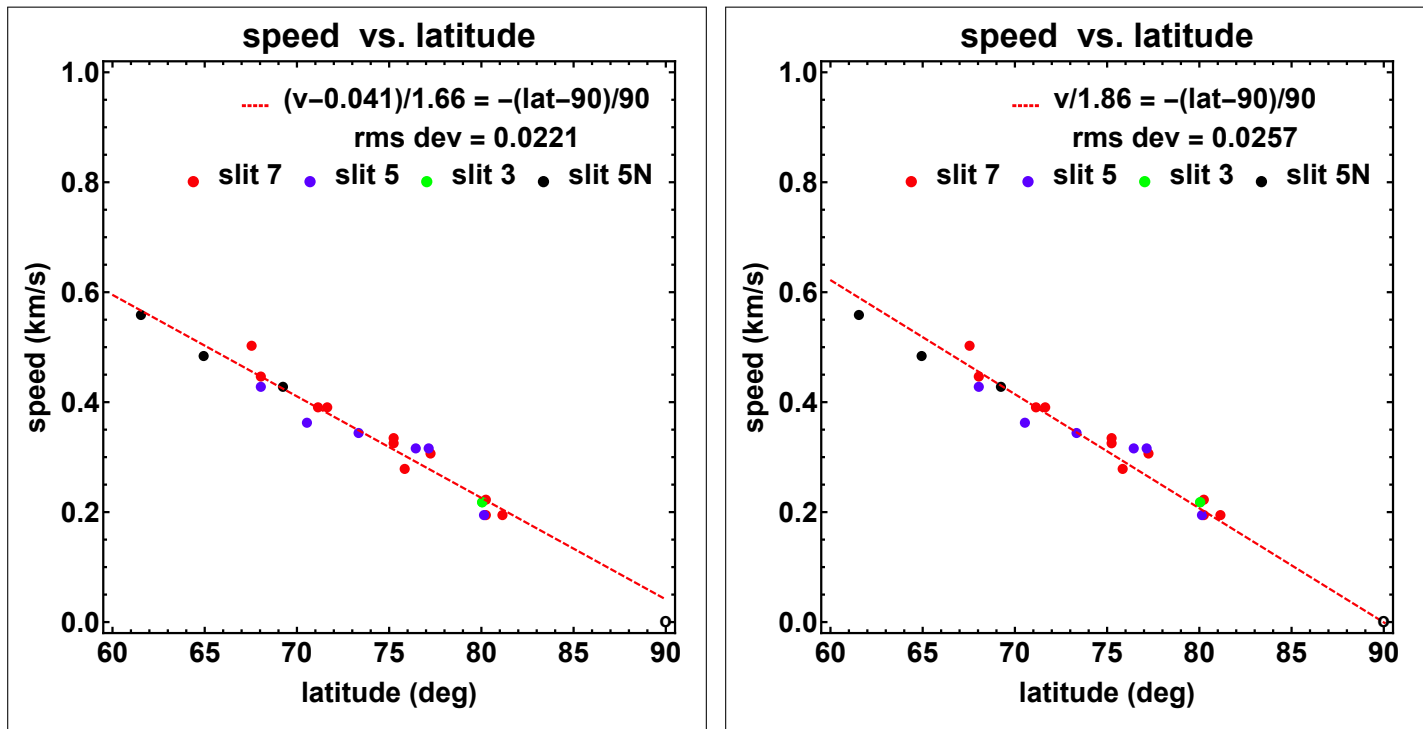


**Figure 7.** Same as Figure 6, but with the addition of 3 measurements of north polar faculae in the 60-70° latitude range with a 5-pixel slit. The resulting straight-line fit is slightly better than the fit obtained without those extra points, and the forced fit has a slightly smaller speed parameter (1.86 km s<sup>-1</sup> compared to 1.90 km s<sup>-1</sup>).

faster. (We can be sure that Eq(8) refers to the synodic rate because it was obtained by tracking solar features. The procedure is analogous to placing a mark on the Sun with a grease pencil and recording the elapsed time until the Sun’s rotation returns that mark to the central meridian as seen from the solar orbiting Earth and SOHO spacecraft.)

#### 4. SUMMARY AND DISCUSSION

It is easy to summarize this work. With the help of ChatGTP, I made space-time maps from SOHO/MDI 6767 Å continuum images of the Sun’s south pole in 7-21 February 1997 and 1998. Those maps showed many parallel tracks produced by the solar rotation of polar faculae. By measuring the slopes of those tracks, I obtained speeds whose values decreased with latitude in the 60-80° range and projected linearly to 0 km s<sup>-1</sup> at the south pole. This gave a constant synodic rotational speed of about 8.6 ° day<sup>-1</sup> in a small polar cap at the Sun’s south pole, as one would expect for a polar asymptote of the Sun’s rotation profile (Sheeley & DeVore 1986). A few measurements of north polar faculae gave values consistent with those obtained for south polar faculae, supporting the idea that the two polar regions rotate at the same rate.

The next question is how do these measurements compare with past measurements of the Sun’s high-latitude rotation. Figure 8 summarizes some of the earlier measurements. The blue dashed curve shows the polar extrapolation of the well-known Snodgrass (1983) rotation profile, and the dashed red curve shows the results of this paper as summarized by Eqs (8) and (9) with  $v_0 = 1.90$  km s<sup>-1</sup>. At the pole, the two curves differ by about 0.9 ° day<sup>-1</sup>, corresponding to synodic rotation periods of about 38 days (Snodgrass) and 42 days (this paper).

The colored dots between these two curves indicate polar faculae measurements by Müller (1954) and Waldmeier (1955). The blue dots of Waldmeier are reasonably well mixed with the pink dots of Muller. The green dots that are nearly coincident with blue dots are Muller’s ‘best measurements’, obtained for especially long-lived faculae. In his paper, Waldmeier (1955) mentions that the point at 80° latitude is ‘significantly less precise than the others due to its high latitude’. By contrast, he says that ‘point 6’ at (9.5° day<sup>-1</sup>, 74° latitude) ‘appears to be particularly reliable’. It is interesting that Muller’s 3 best measurements and Waldmeier’s particularly reliable measurement are consistent with each other and with Waldmeier’s significantly less precise measurement; also, those ‘most reliable’ measurements lie roughly alongside the Snodgrass curve with a slope that is steeper than the more distant red curve that I obtained by tracking polar faculae in 1997-1998.

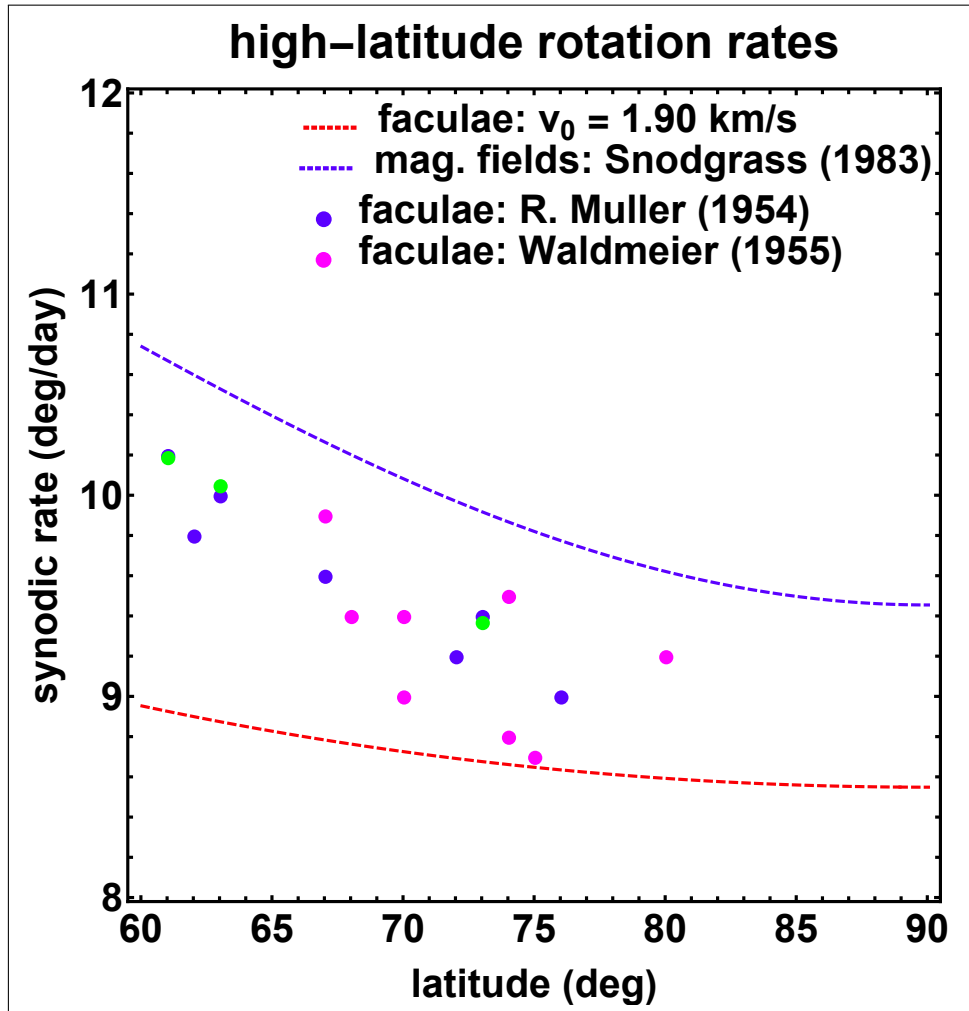


**Figure 8.** A comparison of the synodic rotation rates obtained in this paper with high-latitude measurements obtained previously. The dashed blue curve is a best fit extrapolation of the [Snodgrass \(1983\)](#) tracks of magnetic flux elements, and the dashed red curve refers to the result given in Eqs (8) and (9) of this paper. Previous measurements of polar faculae by [Müller \(1954\)](#) and [Waldmeier \(1955\)](#) are shown in the region between those two curves.

In Figure 8, both sets of data points were obtained in the early 1950s when polar faculae occurred in greater numbers than at any time during the past 100 years ([Sheeley 2008](#)). Mueller observed them between September 1952 and April 1954, and Waldmeier observed them during 1951-1954. By comparison, the measurements described in this paper were obtained in 1997 and 1998 at the end of the last cycle of moderately strong polar fields and modest numbers of polar faculae. Probably the opportunity for such a study would have been less favorable during the sunspot minima of 2009 and 2020 when the polar fields were relatively weak. Similarly, there may have been a reduction in the numbers of polar faculae in the weak sunspot cycles during 1880-1910, which might explain why the Greenwich observers did not find a relation between the sunspot cycle and the numbers of polar faculae in those years ([Dyson 1923](#); [Kiepenheuer 1953](#)).

Despite the good agreement between the high-latitude measurements of [Müller \(1954\)](#) and [Waldmeier \(1955\)](#), those rotation rates do not provide a good match with either the speeds of magnetic tracers observed by [Snodgrass \(1983\)](#) or with the measurements of this paper. One might understand the disagreement with the magnetic flux elements because they were observed with relatively low spatial resolution using the Mount Wilson Observatory (MWO) magnetograph. On the other hand, the images from the SOHO/MDI instrument were free of ground-based seeing conditions and probably had a spatial resolution that was consistently better than that obtained by the 1950s-era ground-based telescopes, especially as the seeing degraded while the faculae were being tracked during each day. Also, in the 1950's, neither Muller nor Waldmeier had digital data that could be processed by computers and analyzed with artificial

intelligence like ChatGPT. But those early observers were known for the high quality of their work, and it seems likely that their polar faculae measurements are fairly accurate. Considering that I used a new and untested technique, it seems more likely that I could have overlooked something that may have caused the discrepancy.

Consequently, I have reexamined several aspects of my measurement procedure. It seemed to make more sense to calculate the linear speeds first, finding a best-fit solution and then converting from linear to angular speed by dividing the solution by  $R_{\odot} \cos \lambda_s$ , the radius of the latitude contours. This would avoid the large amount of scatter that would occur if the measured speeds were divided by a progressively smaller number as  $\cos \lambda_s$  approached 0 at the pole. A linear speed profile that reached 0 km s<sup>-1</sup> at the pole made sense because it offset this  $\cos \lambda_s$  behavior and gave a polar asymptote similar to that found at the equator. So, if there were an error, I would expect it to be a systematic error, perhaps produced in the calibration of the chord distance or the elapsed time. Such a systematic error would change the speeds uniformly without affecting their approach to the pole.

For example, the synoptic rotation rate is very sensitive to the effective latitude used in the the plots of speed versus latitude. If the average latitude,  $\langle \lambda_s \rangle$ , that I used for the plots were 1° too small, it would cause the data points in Figures 5-7 to be 1° too far to the left. Consequently, a correction would shift the points to the right so that a forced fit to those corrected points would increase the value of  $v_0$  to about 2.0 km s<sup>-1</sup>. This would increase the synodic rotation rate,  $\omega$ , from 8.6° day<sup>-1</sup> to 9.0° day<sup>-1</sup>, and place my dashed red curve in the midst of the polar faculae measurements (but with a lower slope than one would infer from those measurements).

There are several ways that these measurements could be improved. First, the space-time slit could be curved so that it fits the shape of the polar latitudes. This might strengthen the tracks, and also allow measurements closer to the pole. Second, one might try using continuum images from the *Solar Dynamics Observatory* (SDO) spacecraft. Presumably, these images were obtained uniformly and at a greater cadence than those obtained with the SOHO/MDI instrument. Also, one could study the effect of  $B_0$  by selecting times that it is 7.25° (for tracking north polar faculae), -7.25° (for tracking south polar faculae), and 0° (when the latitude contours would be straight and well suited for a straight space-time slit.) Possible disadvantages might be a limited number of polar faculae in recent years when the polar fields have been relatively weak, and the need to flat-field the solar images. (Flat fielding might be relatively easy with the help of ChatGPT.) (Since preparing this paper, I learned that Pesnell, Clark, and Barzal made a presentation at the COFFIES workshop, in which they showed a flat-fielded image obtained in the 4500 Å continuum with the Atmospheric Imaging Assembly (AIA) on SDO. The image was created using a ‘progressive standard deviation method’, and showed horizontal lines (or arcs) indicating the positions of polar faculae during the course of a day.) Third, it would be interesting to try using very high spatial resolution like that available with the 4 m Daniel K. Inouye Solar Telescope (DKIST) on Maui, Hawaii or the 1.6 m Goode Solar Telescope at Big Bear Solar Observatory. Such high resolution might allow measurements very close to the pole (or on the other side of the pole that is favorably tipped toward the Earth).

I am grateful to Yi-Ming Wang (NRL) for telling me about the presentations at the 26 June 2024 COFFIES workshop on the ‘Science at the Poles’. I am also grateful to Harry Warren (NRL) for helping me to analyze the 6767 Å continuum images that were obtained by the SOHO/MDI instrument during 1996-2005 and that led to our original paper about the distribution of faculae on the Sun (Sheeley & Warren 2006).

## REFERENCES

- Dyson, F. 1923, MNRAS, 84, 96,  
doi: [10.1093/mnras/84.2.96](https://doi.org/10.1093/mnras/84.2.96)
- Kiepenheuer, K. O. 1953, in *The Sun*, ed. G. P. Kuiper, 322
- Muñoz-Jaramillo, A., Sheeley, N. R., Zhang, J., & DeLuca, E. E. 2012, ApJ, 753, 146,  
doi: [10.1088/0004-637X/753/2/146](https://doi.org/10.1088/0004-637X/753/2/146)
- Müller, R. 1954, ZA, 35, 61
- Sheeley, N. R., J. 1976, J. Geophys. Res., 81, 3462,  
doi: [10.1029/JA081i019p03462](https://doi.org/10.1029/JA081i019p03462)
- . 1991, ApJ, 374, 386, doi: [10.1086/170129](https://doi.org/10.1086/170129)
- . 2008, ApJ, 680, 1553, doi: [10.1086/588251](https://doi.org/10.1086/588251)
- Sheeley, N. R., J., Cooper, T. J., & Anderson, J. R. L. 2011, ApJ, 730, 51, doi: [10.1088/0004-637X/730/1/51](https://doi.org/10.1088/0004-637X/730/1/51)
- Sheeley, N. R., J., & DeVore, C. R. 1986, SoPh, 103, 203,  
doi: [10.1007/BF00147824](https://doi.org/10.1007/BF00147824)
- Sheeley, N. R., J., & Warren, H. P. 2006, ApJ, 641, 611,  
doi: [10.1086/500392](https://doi.org/10.1086/500392)
- Sheeley, Neil R., J. 1964, ApJ, 140, 731,  
doi: [10.1086/147966](https://doi.org/10.1086/147966)
- Sheeley, Neil Rolfson, J. 1965, PhD thesis, California Institute of Technology
- Snodgrass, H. B. 1983, ApJ, 270, 288, doi: [10.1086/161121](https://doi.org/10.1086/161121)
- Waldmeier, M. 1955, ZA, 38, 37